JOURNAL OF GEOPHYSICAL RESEARCH, VOL. 98, NO. D3, PAGES 4919–4930, MARCH 20, 1993

Global Climatologies of Solar Radiation Budgets at the Surface and in the Atmosphere From 5 Years of ERBE Data

ZHANQING LI[1]

Atmospheric Environment Service, Dorval, Quebec, Canada

H. G. LEIGHTON

Department of Atmospheric and Oceanic Sciences, McGill University, Montreal, Quebec, Canada

As a result of recent satellite-based observation programs, knowledge of the radiation budget at the top of the atmosphere has improved substantially. In comparison, there has been little improvement in knowledge of the radiation budgets at the surface and in the atmosphere. Based on a simple parameterization, global climatologies of the solar radiation budget at the surface and in the atmosphere are developed from 5 years of Earth Radiation Budget Experiment data and European Centre for Medium Range Weather Forecasts humidity data. Both data sets have global coverage on 2.5° × 2.5° grids. Global distributions of the solar radiation budget at the surface give maximum seasonal values of the net solar radiation for the subtropical oceans of more than 300 W m^{-2}. The maximum seasonal absorption in the atmosphere is about 120 W m^{-2}. Shortwave cloud forcing at the surface and in the atmosphere is also derived. Clouds reduce the seasonally averaged surface net solar radiation by up to 175 W m^{-2}, whereas they increase seasonal net solar radiation in the atmosphere by less than 15 W m^{-2}. The globally and annually averaged net solar radiation budgets in the atmosphere and at surface are 83 and 157 W m^{-2}, respectively. Expressed as percentages of the solar radiation incident at the top of the atmosphere, these values correspond to a globally and annually averaged absorption in the atmosphere and at the surface of 24.3% and 46.0%, respectively, and a planetary albedo of 29.7%.

1. INTRODUCTION

Measurements of Earth's radiation budget are essential to improve understanding of Earth's climate and climate change. The total radiation budget of the earth-atmosphere system may be considered as consisting of two components, the budget in the atmosphere and the budget at the surface. Knowledge of both of these components, rather than simply the budget of the system as a whole, is important.

Acquisition of a complete picture of the spatial and temporal variation of the radiation budget has been a challenge for a long time. With the advent of satellite observations, knowledge of the radiation budget at the top of atmosphere (TOA) has improved substantially in the last few decades. The major accomplishments achieved by satellite observations and their contributions to studies of Earth's climate have been summarized by *Hartmann et al.* [1986] and *Ramanathan* [1987]. In comparison, little progress has been made in the development of global climatologies of radiation budgets in the atmosphere and at the surface. To a large extent, knowledge of these two budgets is still mainly based on the atlases prepared from surface-based observations [*Budyko*, 1965; *Esbenson and Kushnir*, 1981]. Climatologies determined from surface-based measurements have the obvious shortcomings of limited and inhomogeneous coverage. These shortcomings can, in principle, be overcome by measurements from space. However, there is a major challenge in relating quantities measured from space to the quantities at the surface. Since the 1980s there has been great interest in exploiting the potential of such relationships. One of the goals of the World Climate Research Program is to derive the global surface radiation budget (SRB) from satellite measurements with a accuracy of 10 W m^{-2} for monthly mean fluxes averaged over regions of 250 × 250 km^2 [*Suttles and Ohring*, 1986]. There are still major difficulties in determining the longwave component of the surface radiation budget from space, but considerable progress has been made in determining the shortwave surface radiation budget (SSRB).

Until recently, the majority of techniques derived the insolation at the surface, which is one component of the SSRB [*Schmetz*, 1989]. Global climatologies of surface insolation have been developed by *Raschke et al.* [1987] and *Pinker and Laszlo* [1992] from International Satellite Cloud Climatology Project (ISCCP) reduced data sets. To obtain the SSRB from insolation requires knowledge of surface albedo. This was the approach adopted by *Raschke and Preuss* [1979], who developed the first global measurements of solar radiation budgets in the atmosphere and at the surface from 1 month of NIMBUS 3 measurements. The accumulation of the errors in the estimation of the insolation and albedo limits the usefulness of this approach. In an attempt to find a direct relation between the SSRB and TOA fluxes, *Weare* [1989] looked for correlations between these quantities in the output from a general circulation model and found promising results. Based on radiative transfer calculations, *Cess and Vulis* [1989] and *Cess et al.* [1991] derived a linear relationship between the SSRB and the net solar radiation at the TOA. The major limitation of the relationship was its restriction to clear skies, but the accuracy of the

[1]Now at Canada Centre for Remote Sensing, Ottawa, Ontario, Canada.

Copyright 1993 by the American Geophysical Union.

Paper number 93JD00003.
0148-0227/93/93JD-00003$05.00

method was also limited by its restriction to a limited range of surface types. On the basis of radiative transfer calculations, *Li et al.* [1993*b*] proposed a simple parameterization that is independent of cloud cover and surface type that relates the SSRB to the reflected flux at the TOA. Comparisons of the SSRB deduced by applying the parameterization to Earth Radiation Budget Experiment (ERBE) measurements with surface-based measurements showed good agreement [*Li et al.*, 1993*a*]. This provides more confidence in the application of the parameterization to the 5 years of ERBE data to determine the climatology of the solar radiation budget at the surface. The climatology of the radiation budget in the atmosphere is deduced from the radiation budgets at the TOA and at the surface.

Knowledge of the global climatologies of solar radiation absorbed in the atmosphere and surface allows the determination of the globally averaged annual disposition of solar radiation. Previous studies [*London and Sasamori*, 1971; *Wittman*, 1978; *U.S. National Academy of Science*, 1975] have shown significant differences in the magnitudes of the fractions reflected to space and absorbed in the atmosphere and surface. The present work, with its more complete data, should provide a more reliable estimate of these quantities.

Only selected plots of the SSRB, solar radiation absorbed in the atmosphere, and cloud forcing of the SSRB are presented here. A complete set of figures giving monthly averages of the radiation budgets is available from the authors.

2. ALGORITHM

For the sake of completeness, a brief outline of the algorithm is presented here. Details about the algorithm are given by *Li et al.* [1993*b*]. The algorithm, which is based on results of radiative transfer calculations, is a simple linear relationship:

$$a_s = \alpha(\mu, p) - \beta(\mu, p)r \tag{1}$$

$$A_s = a_s\, d\mu S_0 \tag{2}$$

where a_s is the fraction of the solar irradiance incident at the TOA that is absorbed at the surface, A_s is the irradiance absorbed at the surface, d is the correction to the mean Sun-Earth distance, μ is the cosine of solar zenith angle, r is the local planetary albedo, and S_0 is the solar constant. The value of S_0 is taken to be 1365 W m^{-2}, the value used in ERBE. Both intercept α and slope β are parameterized in terms of μ and precipitable water p (cm) as follows:

$$\alpha(\mu, p) = \alpha_0(\mu) + \Delta\alpha(\mu, p) \tag{3}$$

$$\alpha_0(\mu) = 1 - \left[\left(\frac{C}{\mu} + \frac{D}{\mu^{1/2}}\right)\right] \tag{4}$$

$$\Delta\alpha(\mu, p) = \frac{1}{\mu}\,[1 - \exp(-\mu)][0.0699 - 0.0683(p)^{1/2}] \tag{5}$$

$$\beta(\mu, p) = \beta_0(\mu) + \Delta\beta(p) \tag{6}$$

$$\beta_0(\mu) = 1 + (A + B \ln \mu) \tag{7}$$

$$\Delta\beta(p) = -0.0273 + 0.0216(p)^{1/2} \tag{8}$$

Different sets of values of the coefficients A, B, C, and D were obtained for clear skies and for different cloud types. The differences, however, between the various sets of coefficients were small, implying that the relationship is almost independent of cloud amount, type and thickness, and surface type. The relationship defined by the above equations was substantiated by comparisons with measurements taken from a meteorological tower located at Boulder, Colorado. Using the single set of parameters of the clear model ($A = 0.0815$; $B = 0.0139$; $C = -0.01124$; $D = 0.1487$), the absolute and relative mean errors in the estimates of surface absorbed flux are -2.5 W m^{-2} and -0.4% for 54 sets of clear sky observations and -1.1 W m^{-2} and -0.2% for 239 observations taken without regard to sky condition. Similar agreement is obtained with data collected from a tower near Saskatoon, Saskatchewan, in winter when the surface is covered by snow [*Li et al.*, 1993*a*].

Since the algorithm was derived from the results of radiative transfer calculations for specific solar zenith angles, it is necessary to demonstrate that the algorithm is applicable to the determination of the daily mean SSRB. To this end, (1) and (2) may be written as

$$A_s = A_0(\mu, p) - \beta(\mu, p)R \tag{9}$$

$$A_0(\mu, p) = dS_0\mu\alpha(\mu, p) \tag{10}$$

$$R(\mu) = dS_0\mu r \tag{11}$$

where R is the reflected flux at the top of the atmosphere. Since A_0 and β depend on μ, it is not necessarily true that for averages over a day or a month that

$$\bar{A}_s = A_0(\bar{\mu}, p) - \beta(\bar{\mu}, p)\bar{R} \tag{12}$$

where $\bar{\mu}$ is the time-averaged value of μ. Except for small values of μ, in which case the net flux at the surface will be small, A_0 is a linear function of μ [see *Li et al.*, 1993*b*, Figure 16]. This suggests that replacing $\bar{A}_0$ by $A_0(\bar{\mu})$ is a good approximation. A similar conclusion holds for the dependence of β on μ (see curve 1 in Figure 15 of *Li et al.* [1993*b*]). To verify (12) explicitly, $\bar{A}_s$ was evaluated from the time average over a day of the instantaneous values of A_s determined from (9) and from (12) with $\bar{R}$ being the time average of the calculated values of R. Pairs of values of $\bar{A}_s$ were determined for all seasons, a broad range of latitudes, column water vapor amounts of 1 and 5 cm, surfaces varying from ocean to fresh snow, and cloud optical thicknesses varying from 0 to 40. The difference between the daily averages was almost always less than 5 W m^{-2} and never larger than 7 W m^{-2}, the values determined from (12) being smaller than the value determined from the averages of the instantaneous values of the net surface flux.

3. DATA

3.1. *ERBE Satellite Data*

The Earth Radiation Budget Experiment provided the most comprehensive observation system for the monitoring of the Earth radiation budget. Three satellites were involved: ERBS in a precessing orbit with an inclination of 57° and NOAA 9 and NOAA 10 in polar orbits with inclinations of 98°. Each satellite carried two packages of scanning and nonscanning radiometers measuring shortwave, longwave,

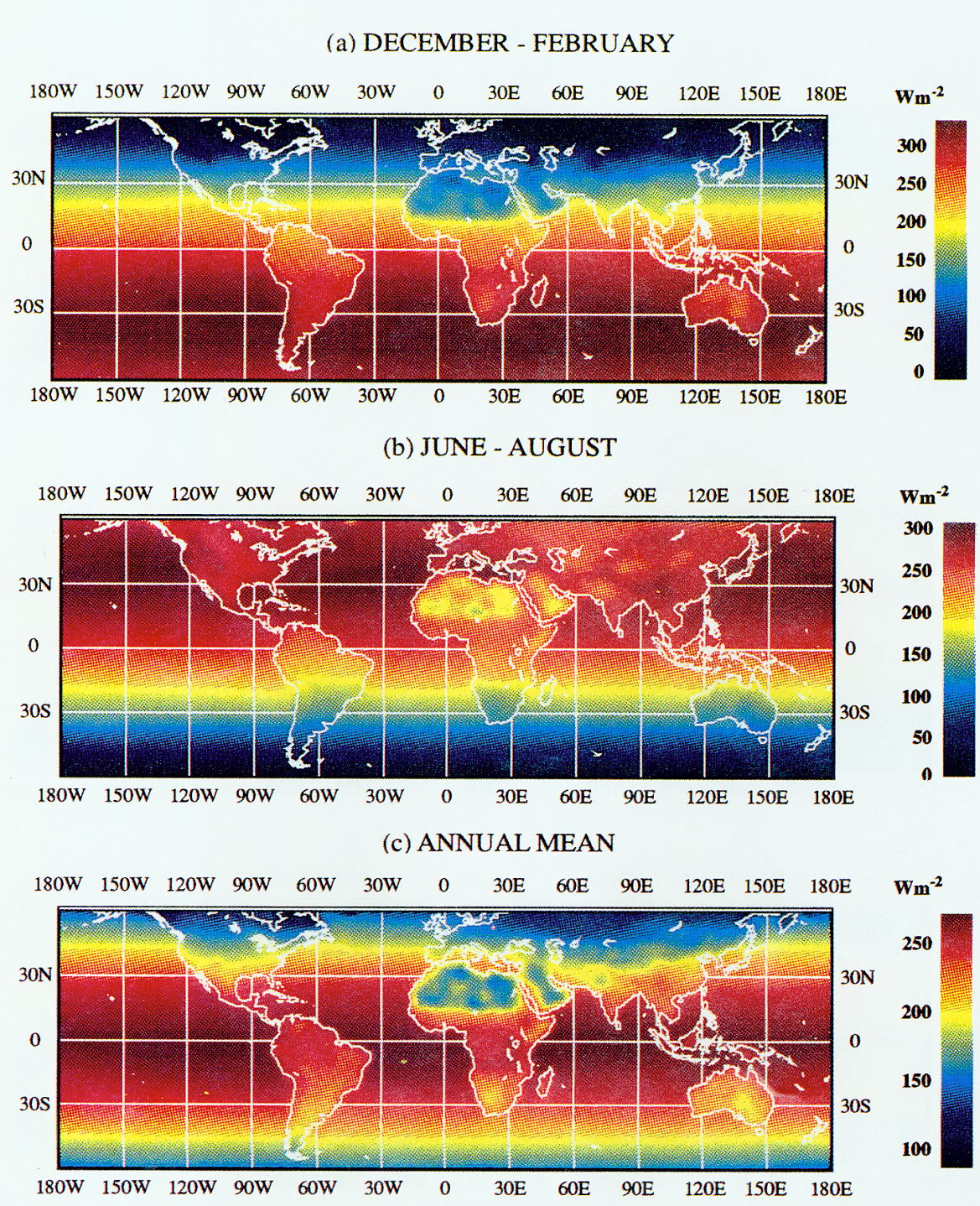

Plate 1. Surface solar radiation budgets under clear skies for the period November 1984 to December 1989: (*a*) December–February, (*b*) June–August, (*c*) annual.

and total outgoing radiation. The nadir footprints were 31 × 47 km^2 for the ERBS scanners and 44 × 65 km^2 for the NOAA scanners. The ERBE data are capable of providing sufficient spatial, temporal, and diurnal sampling to measure the radiation budget of Earth [*Barkstrom and Smith*, 1986].

The data employed in this study come from one of the ERBE products, namely, the regional, zonal, and global averages product designated as the S-4 data. It contains the time and space averages of all the individual estimates of radiant exitance for clear and all sky conditions at the TOA for each month and each spacecraft, as well as from combinations from more than one spacecraft [*NASA Langley Research Center*, 1985]. Although daily mean values are available, monthly mean values of the reflected flux and μ averaged over 2.5° × 2.5° latitude-longitude grids are used. The periods when ERBE S-4 data are available are Novem-

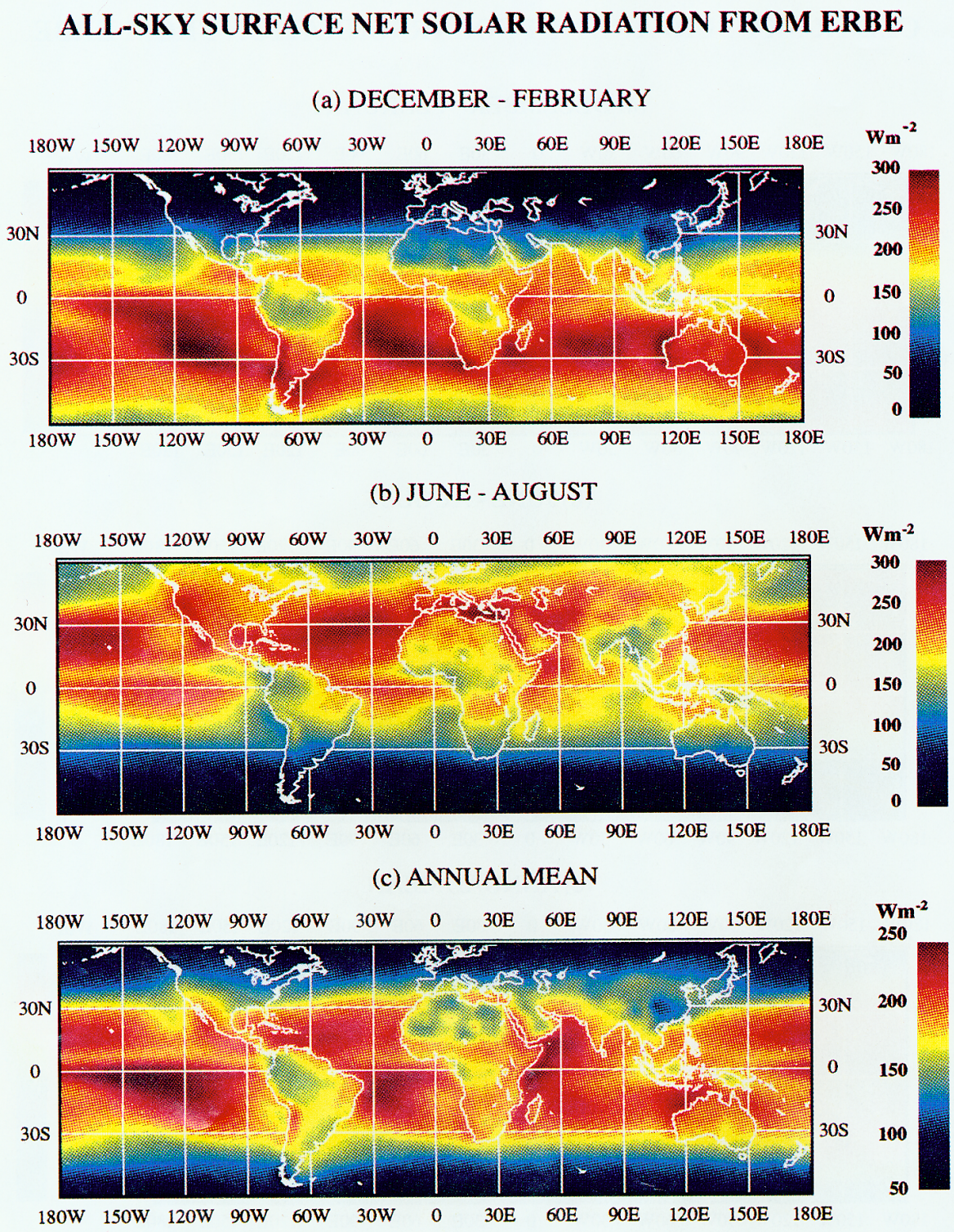

Plate 2. As Plate 1 but for all skies.

ber 1984 to December 1989 for ERBS, February 1985 to January 1987 for NOAA 9, and October 1986 to December 1988 for NOAA 10. Thus there are more than 5 years of data from ERBS and nearly 4 years of global data coverage from NOAA 9 and NOAA 10. To minimize the uncertainty resulting from insufficient diurnal sampling, the product that combines data from more than one satellite is used whenever possible. The product from a single satellite is only employed if no combined data are available, such as over the polar regions which can only be observed by polar orbiting satellites and in 1989 when only ERBS was still functioning.

3.2. *ECMWF Humidity Data*

Apart from the local planetary albedo and the solar zenith angle, the only other input that must be provided is precipitable

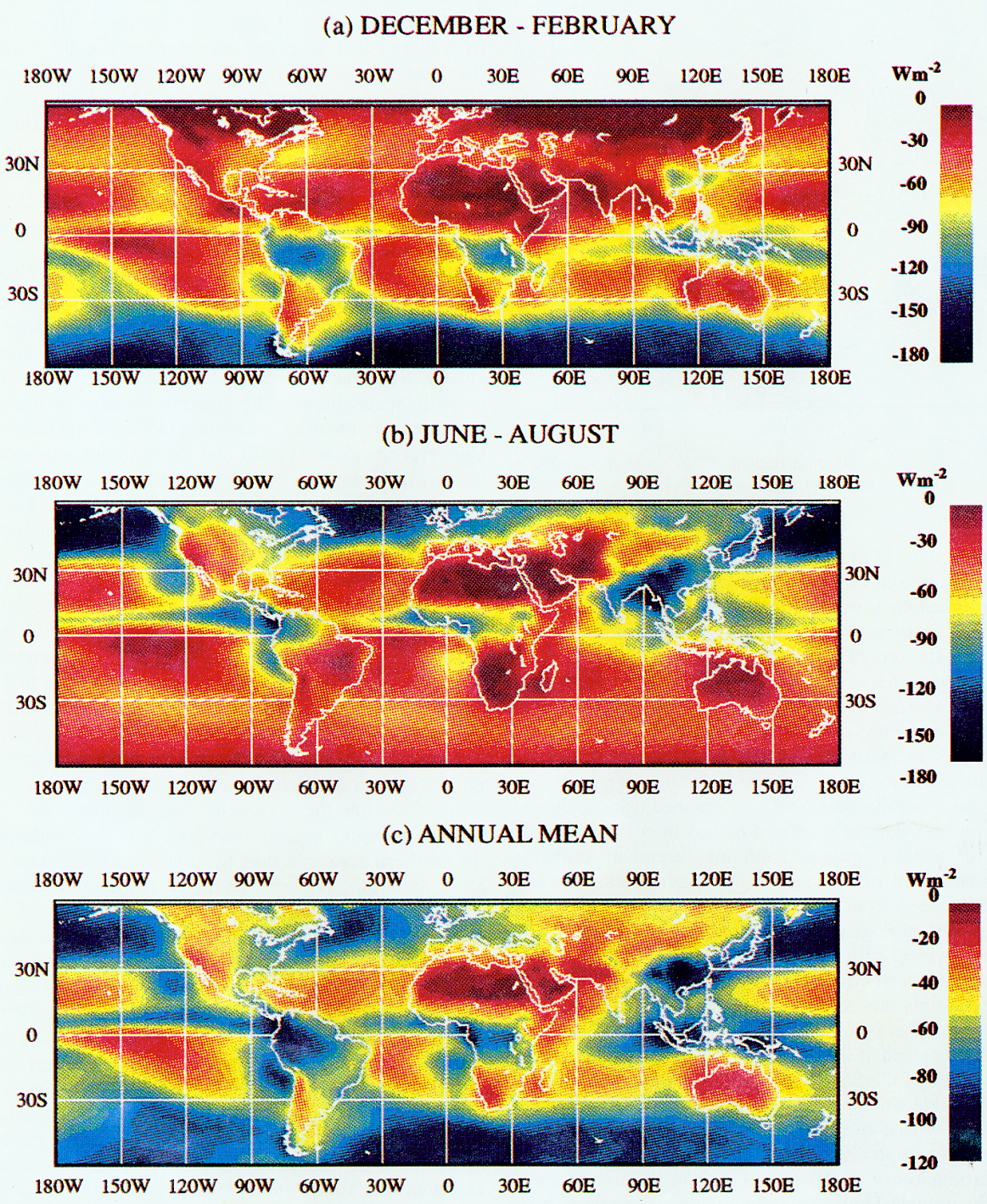

Plate 3. Shortwave cloud forcing at the surface, defined as the difference in the surface radiation budget under all skies and clear skies: (*a*) December–January, (*b*) June–August, (*c*) annual.

water. To match the ERBE data, precipitable water should be available on a regular grid covering the whole globe. The European Centre for Medium-Range Weather Forecast (ECMWF) World Meteorological Organization (WMO) Global Analysis Dataset produced by the ECMWF is a suitable data set for this study. It contains global analyses of temperature, wind, vertical velocity, relative humidity, and geopotential height at seven pressure levels, 1000, 850, 700, 500, 300, 200, and 100 mbar. The horizontal resolution is 2.5° × 2.5°, the same as that of the ERBE data. The analyses are available twice a day, at 0000 UT and 1200 UT, from 1980 through 1989 [*Bengtsson et al.*, 1982]. The humidity file, which is of main interest to us, is obtained by making use of global radiosonde observations, remote sensing data from satellites, and modeling results, together with a data assimilation scheme. Since ECMWF data do not contain surface pressure data, global

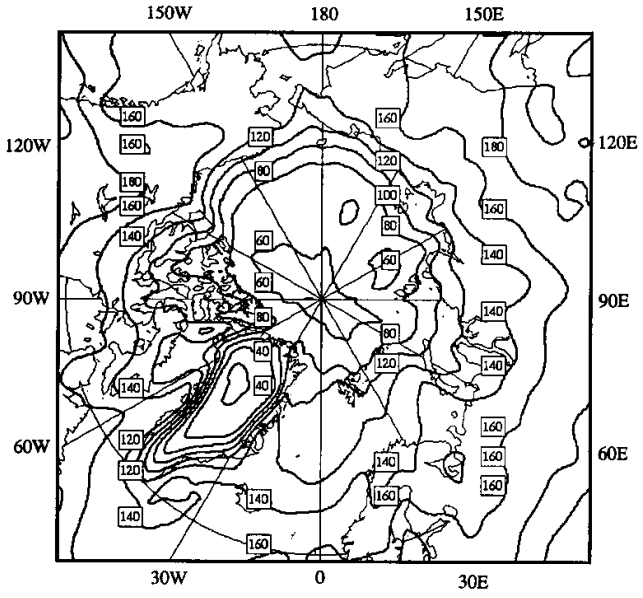

Fig. 1. Surface solar radiation budget (W m^{-2}) in the Arctic in June–August for the years 1985–1988.

topographic data from the Canadian Meteorological Centre [*Pellerin and Benoit*, 1987] are employed to deduce the surface pressure. Precipitable water is determined at each analysis time by vertically integrating the humidity profile from the surface pressure to the top of the atmosphere. Daily and monthly means are obtained by averaging. It is the monthly mean values of precipitable water that are used in the parameterization to determine the monthly mean SSRB. The use of monthly mean values of precipitable water is justified by the weak sensitivity of the surface absorbed flux to the column water vapor. At Boulder the monthly mean SSRB determined using daily and monthly mean values of p differed by less than 1%.

Lack of suitable ground truth measurements prevents direct assessment of the quality of the analyses. *Lambert* [1988] concluded from comparisons of ECMWF and U.S. National Meteorological Center analyses for January and July that a typical daily analysis of relative humidity is only reliable for the northern hemisphere mid-latitudes in January and that monthly means are reliable only in the mid-latitudes of both hemispheres in both months. This is not a satisfactory situation, and it is inevitable that some errors in the determination of the SSRB will be due to the uncertainty in the precipitable water. However, as mentioned above, simulations show that the flux absorbed at the surface is not very sensitive to precipitable water. In fact, the uncertainty in the estimation of SSRB resulting from the use of zonal mean climatological values of precipitable water ranges from 0 to 20 W m^{-2} as solar zenith angle changes from 90° to 0° [*Li et al.*, 1993*b*].

4. BUDGETS

4.1. *Global Budgets*

Plate 1 presents the distribution of the SSRB from 60°S to 60°N under clear skies. It is obtained by averaging the monthly values of SSRB at each grid point over 5 years. The majority of grid points have monthly mean cloud-free values of the SSRB for at least 3 of the 5 years. However, there are a few grid points (approximately 20 out of 7105 grid points) where clear skies are never observed for a particular month in the 5 years of data. Where this happens, the mean of the values at adjacent grid points is substituted. It is apparent from Plate 1 that the prime influences on the distribution are the insolation at the TOA and the contrast in the surface albedo between the land and ocean. This results in a highly zonal pattern with discontinuities at coastlines. During the southern hemisphere summer, maximum values are in the oceans at about 35°S and exceed 330 W m^{-2}. In the northern hemisphere summer, maximum values are about 25 W m^{-2} less. The great desert regions with their high surface albedos stand out as relative minima.

Plate 2 shows the distribution of the SSRB with no discrimination according to sky condition. The main features of the patterns are those that are expected. The large values associated with subtropical highs over oceans stand out clearly. Seasonally averaged maxima are about 300 W m^{-2} in both hemispheres. The relative minima in the tropics correspond to the thick, persistent clouds of the Intertropical Convergence Zone (ITCZ) and the summer monsoon over southeast Asia. Low values off the coast of California are associated with persistent stratocumulus clouds. Low pressures in winter over SW China account for the minimum in the SSRB in this region.

Esbensen and Kushnir [1981] give plots of the SSRB over the oceans from marine observations. While the main features of the present results and those of Esbensen and Kushnir are in accord, there are significant differences in the magnitudes. For example, Esbensen and Kushnir find only a small region over the southern oceans near the southern tip of Africa with SSRB in December to February greater than 270 W m^{-2}, whereas the present results indicate large portions of the southern oceans have SSRB greater than 270 W m^{-2} during these months and, as mentioned above, maximum values greater than 300 W m^{-2}. Similarly, over the northern oceans in June to August the present results are about 30 W m^{-2} greater than the corresponding results from Esbensen and Kushnir.

To isolate the effect of cloud on surface net solar radiation, the difference in the SSRB under all-sky conditions and under clear skies only is computed (Plate 3). This quantity is the surface equivalent of the TOA shortwave (SW) cloud forcing and will be referred to as surface SW cloud forcing. This quantity is always negative and has minimum values of about -180 W m^{-2} at the southern hemisphere oceans and -160 W m^{-2} in the northern hemisphere summer along the storm tracks over the oceans. Other noticeable minima are associated with the summer monsoon in SE Asia, the ITCZ, and southern China in the winter, the same regions that showed minima in the SSRB. The winter storm tracks over the North Atlantic and the North Pacific are also clearly visible. On an annual basis, surface cloud forcing has its maximum values (smallest absolute values) over the major desert regions and over the tropical Pacific where values exceed -20 W m^{-2}.

Chertock et al. [1991] present results of the surface SW cloud radiative forcing for January and July, based on 7 years of Nimbus 7 data. They find a minimum value of -210 W m^{-2} in the North Pacific in July compared to a minimum of about -160 W m^{-2} in the present work for the average from June to August. Apart from this, as well as can be

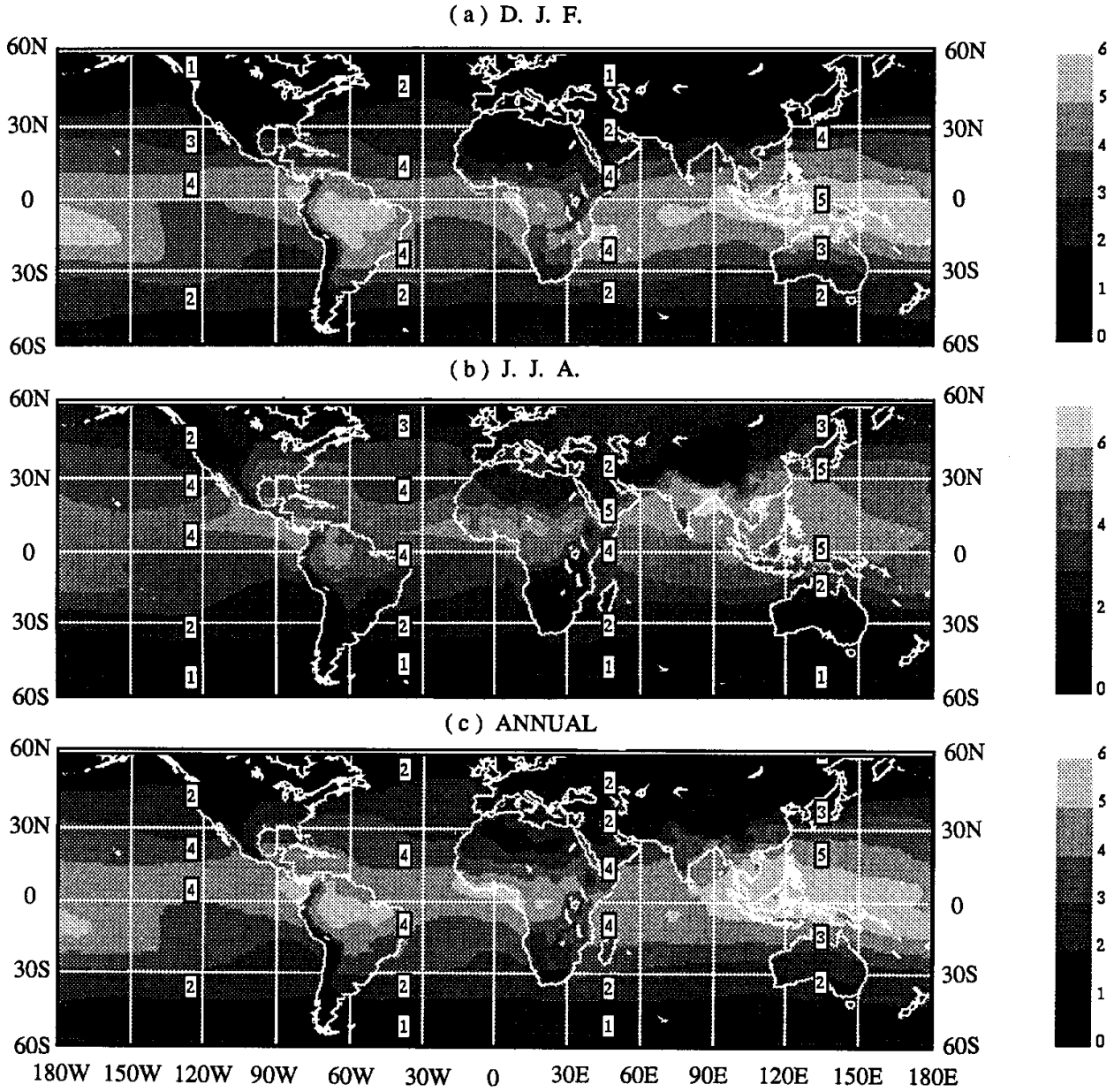

Fig. 2. Precipitable water (cm) from ECMWF analyses for the period 1985–1989: (*a*) December–February, (*b*) June–August, (*c*) annual.

ascertained from comparisons of the plots, the results compare very well.

Figure 1 shows a contour map of the summer SSRB in the Arctic under all-sky conditions. Since the ERBE scene identification over snow- and ice-covered regions is very unreliable [*Li and Leighton*, 1991], no attempt is made to deduce clear sky budgets. The main feature is the region of low values with a minimum of less than 20 W m^{-2} over the Greenland ice cap and the tight gradient along the Greenland coast. Elsewhere, the pattern is more or less zonal. The annual average shows a similar pattern but with values that are typically a factor of 2 smaller. The distributions agree well with the results of *Vowinckel and Orvig* [1964] from surface observations but with local differences of as much as 40 W m^{-2}. The distribution in the Antarctic is more zonal but of similar magnitude to the Arctic distribution.

Absorption in the atmosphere is deduced from the difference between the TOA net flux and the SSRB. Figure 2 shows the water vapor distributions averaged over the summer and winter months and over the whole year. The corresponding absorption in the atmosphere is shown in Plate 4. The influence of the water vapor distribution on the atmospheric absorption is very clear. Maxima of water vapor over Indonesia, the Congo, and northern Brazil stand out clearly in the plots of atmospheric absorption. Likewise, the low water vapor amounts over the Andes result in a distinct minimum in atmospheric absorption. However, the relatively small water vapor amounts over the Sahara in winter do not produce a comparable pattern in the atmospheric absorption, presumably because of the relatively high surface albedo resulting in additional solar radiation available for atmospheric absorption. The distribution of

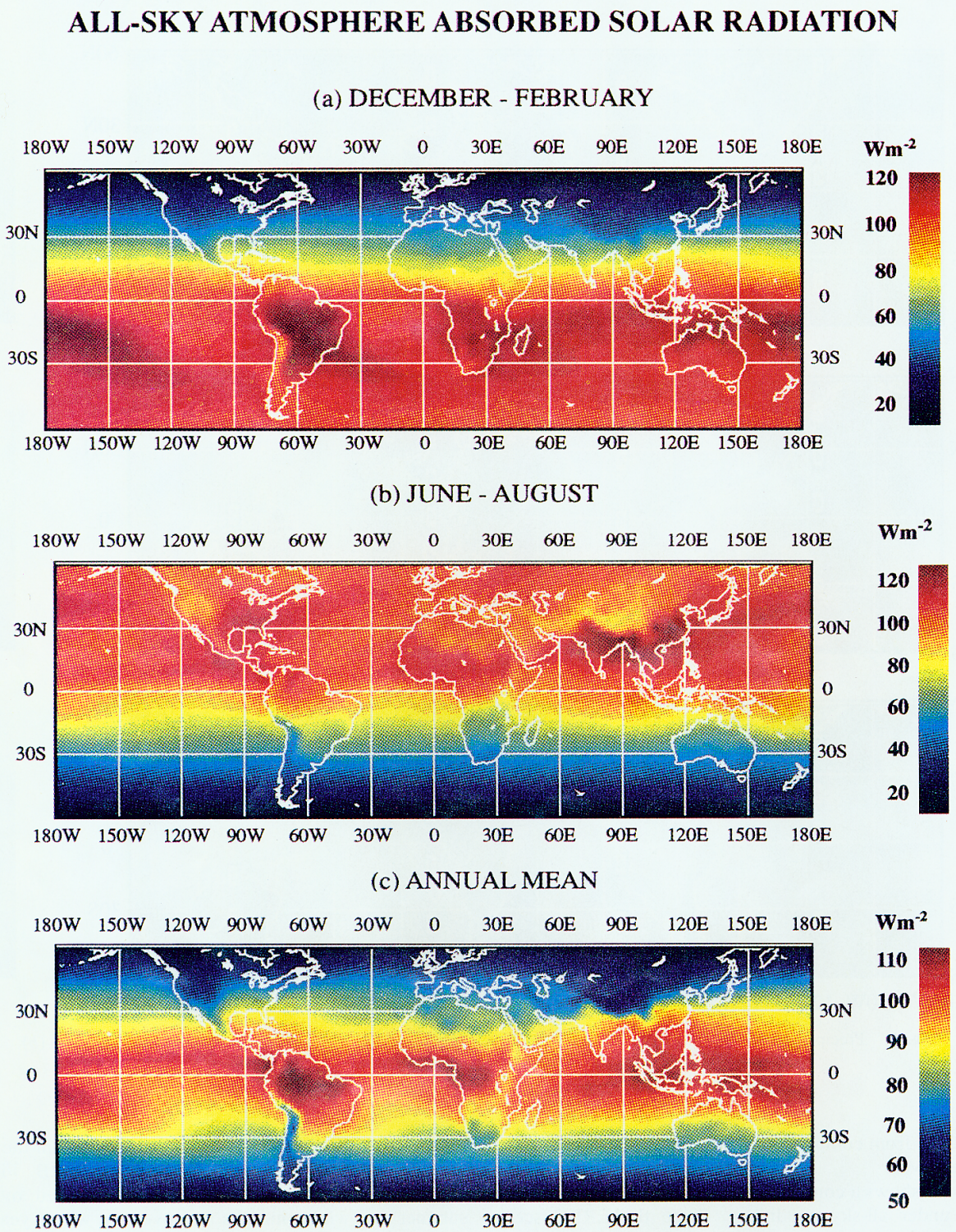

Plate 4. Solar radiation absorbed in the atmosphere for the period November 1984 to December 1989: (*a*) December–February, (*b*) June–August, (*c*) annual.

atmospheric absorption for clear skies is very similar to that found for the full data set. The difference between the all-skies and clear-skies absorption is shown in Plate 5. Differences almost everywhere are less than 10 W m^{-2}, the largest values in December to February being over the Amazon basin and in June to August being over SE Asia and the storm tracks of the North Pacific.

Over the polar regions, in addition to water vapor amount, the flux absorbed in the atmosphere in summer is influenced by the length of the polar day and the albedo of the underlying surface. As shown in Figure 3, the pattern of absorbed radiation is quite zonal, increasing slightly towards the poles, with the notable exception in the arctic of the influence of the Greenland ice cap. It is interesting to note that the combined effect of the factors mentioned above results in a minimum over the southern tip of Greenland.

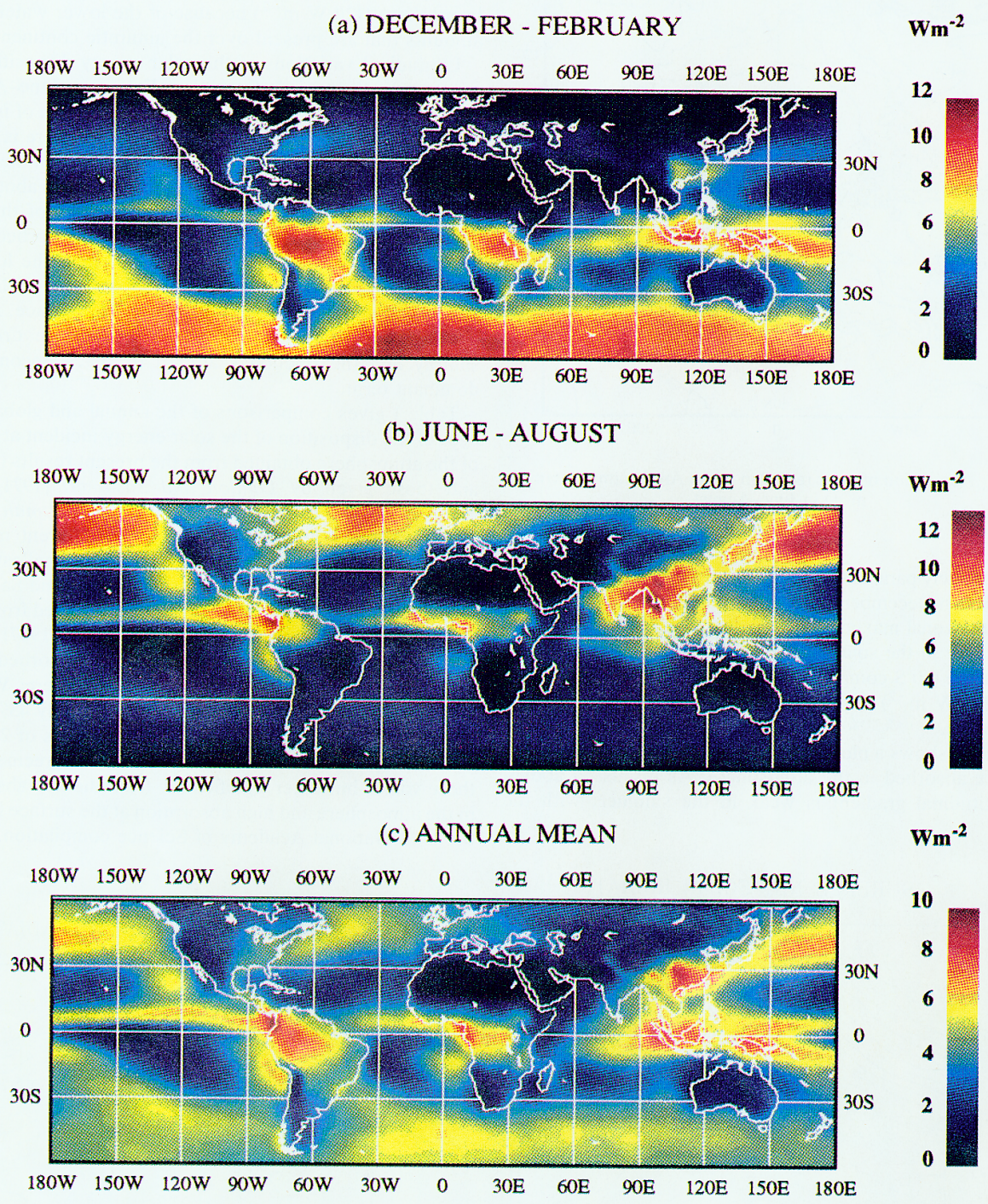

Plate 5. Difference in absorption of solar radiation in the atmosphere for all skies and clear skies: (*a*) December–February, (*b*) June–August, (*c*) annual.

4.2. *Zonal and Global Average Budgets*

One of the potential uses of the results presented here is to verify results from global climate models. Although it is necessary that these models reproduce correctly the global distribution of the solar radiation budgets, a more convenient set of quantities for comparison purposes are the zonally averaged budgets. Figure 4 shows the SSRB as a function of latitude and month. The paths of the variation of the latitude of the maximum SSRB with time in each hemisphere are depicted by the two dashed curves. In the northern hemisphere, the latitude of the maximum shifts gradually from the equator in December to about 30°N in July, and the magnitude of the zonal maximum changes from 200 W m^{-2} to more than 240 W m^{-2}. In the southern hemisphere, the track of the maximum is

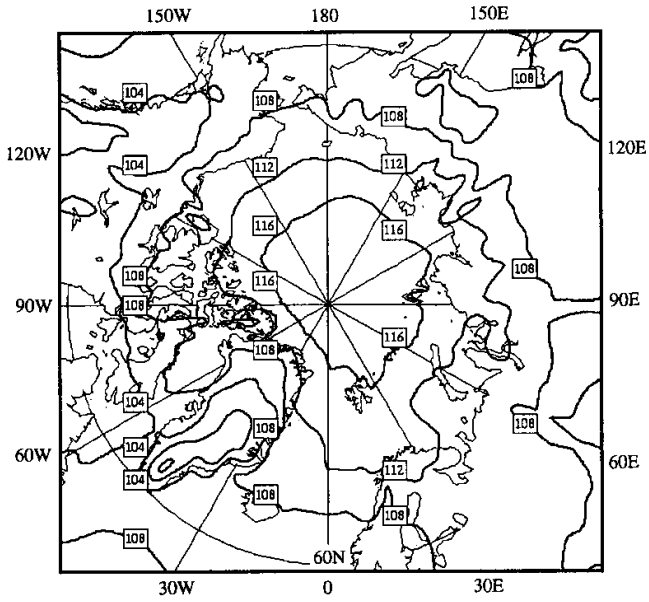

Fig. 3. Absorption of solar radiation in the Arctic atmosphere (W m^{-2}) in June–August.

approximately parallel to that in the northern hemisphere, i.e., from 30°S in December to the equator in June. The latitude at which the zonal maximum is largest is displaced farther from the equator in the southern hemisphere than in the northern hemisphere (30°S compared to 20°N) and has a larger magnitude (260 W m^{-2}) due to the larger ocean area in southern hemisphere.

Figure 5 shows a plot equivalent to that of Figure 4 but for the flux absorbed in the atmosphere. As discussed above, the latitudinal gradient is weak in the summer, with the greatest values of the zonal averages occurring at high latitudes. The maximum zonal average in the northern hemisphere (130 W m^{-2}) is greater than in the southern hemisphere (120 W m^{-2}) because of the lower water vapor amounts that are present over the antarctic continent.

Latitudinal variations of the solar energy disposition averaged over the periods December–February, June–August, and annually are shown in Figure 6. The fraction of incident solar radiation that is absorbed in the atmosphere is almost independent of latitude except at high latitudes in the winter hemisphere where it increases from about 24% to about 30%, presumably due to the increased path length of the solar beam. The fractions scattered to space and absorbed at the surface show strong latitudinal variations. In the low latitudes, absorption at the surface is about twice as large as absorption in the atmosphere or scattering to space. At high latitudes the fraction absorbed at the surface drops off sharply and the fraction scattered to space becomes the dominant term.

Table 1 gives comparisons of the annual and global averages of the disposition of the solar energy incident at the top of the atmosphere obtained from the present results (ERBE) and those given by *London and Sasamori* [1971], *U.S. National Academy of Science* [1975], and *Wittman* [1978]. The planetary albedos obtained by the different methods agree well; the range between the largest and smallest values being 3.3%. Except for the results of London and Sasamori, they all lie within the range of 29–31% determined from other satellite based measurements [*Ramanathan*, 1987]. There are, however, large variations in how the absorbed flux is divided between the surface and the atmosphere. Wittman gives 26% absorbed in the atmosphere and only 43% at the surface, and London and Sasamori give values of 22% and 45%. The present results are in reasonable agreement with these values but differ significantly from the low absorption in the atmosphere and high absorption at the surface found in the U.S. National Academy of Science compilation.

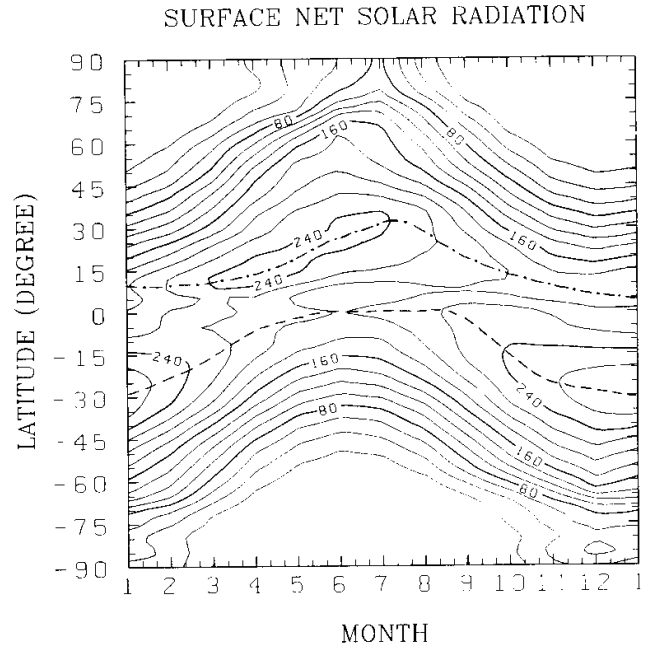

Fig. 4. Monthly and latitudinal variation of absorption of solar radiation at the surface. The dashed lines show the latitude of maximum absorption in each hemisphere.

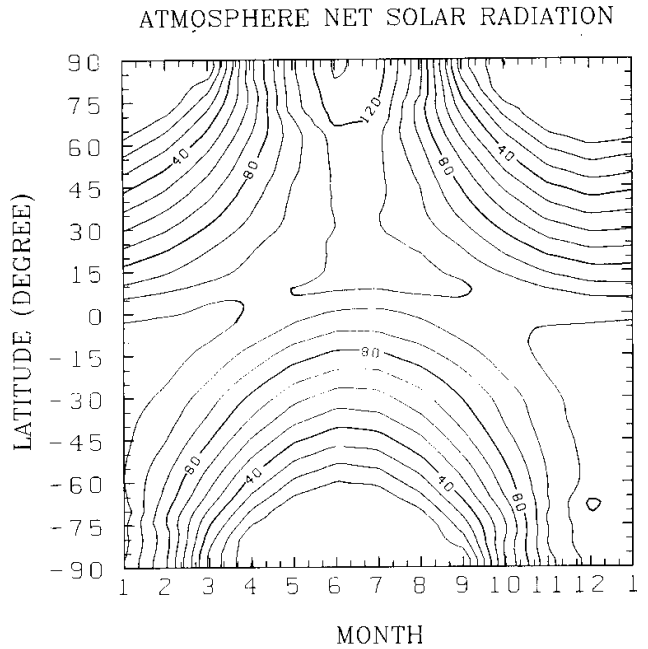

Fig. 5. As Figure 4 but for absorption in the atmosphere.

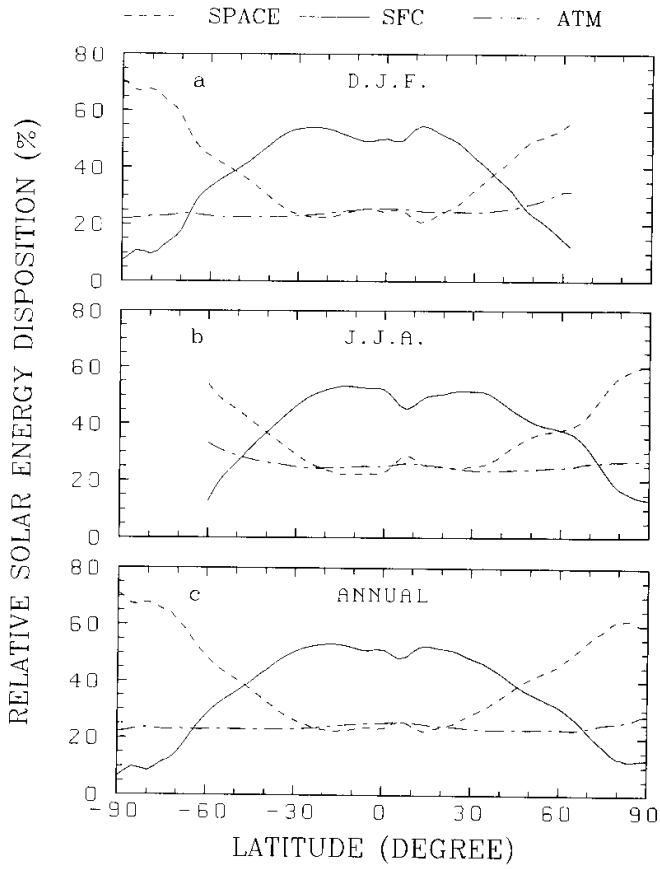

Fig. 6. Latitudinal variation of the relative disposition of the incident solar radiation: (*a*) December–February, (*b*) June–August, (*c*) annual.

In addition to the global mean budgets, hemispherical means may also be compared with earlier estimates. Table 2 shows a comparison of the present results for the northern hemisphere with the results of *Houghton* [1954] and *London* [1957] and for the southern hemisphere with the results of *Sasamori et al.* [1972]. The present results have a lower hemispheric albedo than was found from the calculations of Houghton and of London and significantly higher absorption in the atmosphere. The absorption at the surface is only slightly less than the values found from the calculations. For the southern hemisphere, the present results give a substantially smaller hemispheric albedo than was found by Sasamori and greater absorption both in the atmosphere and at the surface.

The present results show little monthly variation in the solar energy disposition, the monthly values always lying within 1.5% of the annual mean values.

TABLE 1. Annual and Global Average of the Disposition of Solar Energy Incident at the Top of the Atmosphere

Source	Space	Atmosphere	Surface
ERBE	29.7	24.3	46.0
Wittman [1978][a]	31	26	43
U.S. National Academy of Sciences [1975][b]	30	19	51
London and Sasamori [1972]	33	22	45

In percent.
[a]Taken from *Liou* [1980].
[b]Taken from *Wallace and Hobbs* [1977].

TABLE 2. Annual Average Hemispherical Disposition of Solar Energy Incident on the Top of the Atmosphere

Source	Space	Atmosphere	Surface
Northern Hemisphere			
ERBE	30.1	24.4	45.5
Houghton [1954][a]	34	19	47
London [1957][a]	35.2	17.4	47.4
Southern Hemisphere			
ERBE	29.1	24.4	46.5
Sasamori et al. [1972][a]	35	21	45

In percent.
[a]Taken from *Liou* [1980].

5. SUMMARY

A simple linear relationship [*Li et al.*, 1993*b*] that is based on radiative transfer calculations has been applied to 5 years of ERBE data to deduce monthly averages of the net solar radiation absorbed at the surface and in the atmosphere averaged over 2.5° × 2.5° regions. The method requires monthly averaged values of the precipitable water, but does not require scene identification, knowledge of the surface albedo, or estimation of cloud properties. The relationship has been validated by comparisons between the net radiation absorbed at the surface deduced from ERBS data and tower measurements, the mean bias error being less than 3 W m^{-2} [*Li et al.*, 1993*a*].

The global radiation budgets determined in the present work show all of the expected features. Quantitatively, the net surface solar radiation agrees moderately well with the distributions over the oceans determined by *Esbensen and Kushnir* [1981], but monthly mean differences are as large as 30 W m^{-2}. Differences in the arctic between the present results and the results given by *Vowinckel and Orvig* [1964] are as much as 40 W m^{-2}. Comparisons of the cloud forcing of the net solar radiation at the surface also show generally good agreement with the recent results of *Chertock et al.* [1991] but local differences are again as large as 50 W m^{-2}. The globally averaged annual disposition of the solar radiation incident at the top of the atmosphere was also determined and the values were found to lie in between results quoted by *Liou* [1980] and *Wallace and Hobbs* [1977].

The results presented here provide the first long-term, satellite-based global climatology of the solar radiation budgets at the surface and in the atmosphere with fine and homogeneous spatial and temporal resolution. They should be of great advantage for diagnosing clouds and evaluating radiation transfer calculations in general circulation models. They may also be useful in studies of the energy exchanges at the surface.

Acknowledgments. This research is supported by a Natural Sciences and Engineering Research Council (NSERC) of Canada Visiting Fellowship awarded to Z.L. and research grants to H.L. from NSERC and the Canadian Atmospheric Environment Service. We are grateful to L. Garand, H. Barker, and C. Grassotti for their comments and to J. Sheng for help with the data processing. Data were kindly provided by R. Davies and R. Benoit. The help of Y.

Chartier and M. Lepine in producing the computer plots is very much appreciated.

REFERENCES

Barkstrom, B. R., and G. L. Smith, The Earth radiation budget experiment: Science and implementation, *Rev. Geophys.*, *24*, 379–390, 1986.

Bengtsson, L., M. Kanamitsu, P. Kallberg, and S. Uppala, FGGE 4 dimensional data assimilation at ECMWF, *Bull. Am. Meteorol. Soc.*, *63*, 29–43, 1982.

Budyko, M. I., *The Heat Balance of the Earth's Surface*, 259 pp., U.S. Department of Commerce, Washington, D. C., 1965.

Cess, R. D., and I. L. Vulis, Inferring surface solar absorption from broadband satellite measurements, *J. Clim.*, *2*, 974–985, 1989.

Cess, R. D., E. G. Dutton, J. J. DeLuisi, and F. Jiang, Determining surface solar absorption from broadband satellite measurements for clear skies: Comparison with surface measurements, *J. Clim.*, *4*, 236–247, 1991.

Chertock, B., R. Frouin, and R. C. J. Somerville, Global monitoring of net solar irradiance at the ocean surface: Climatological variability and the 1982–1983 El Nino, *J. Clim.*, *4*, 639–650, 1991.

Esbensen, S. K., and Y. Kushnir, The heat budget of the global ocean: An atlas based on estimates from surface marine observations, *Rep. 29*, 27 pp., Clim. Res. Inst., Oreg. State Univ., Corvallis, 1981.

Hartmann, D. L., V. Ramanathan, A. Berroir, and G. E. Hunt, Earth radiation budget data and climate research, *Rev. Geophys.*, *24*, 439–468, 1986.

Houghton, H. G., On the annual heat balance of the northern hemisphere, *J. Meteorol.*, *11*, 1–9, 1954.

Lambert, S. J., A comparison of operational global analyses from the European Centre for Medium Range Weather Forcasts (ECMWF) and the National Meteorological Center (NMC), *Tellus*, *40A*, 272–284, 1988.

Li, Z., and H. G. Leighton, Scene identification and its effect on cloud radiative forcing in the arctic, *J. Geophys. Res.*, *96*, 9175–9188, 1991.

Li, Z., H. G. Leighton, and R. D. Cess, Surface net solar radiation estimated from satellite measurements: Comparisons with tower observations, *J. Clim.*, in press, 1993*a*.

Li, Z., H. G. Leighton, K. Masuda, and T. Takashima, Estimation of SW flux absorbed at the surface from TOA reflected flux, *J. Clim.*, *6*, 317–330, 1993*b*.

Liou, K. N., *An Introduction to Atmospheric Radiation*, 392 pp., Academic, San Diego, Calif., 1980.

London, J., A study of the atmospheric heat balance, 75 pp., New York Univ., New York, 1957.

London, J., and T. Sasamori, Radiative budget of the atmosphere, in *Man's Impact on the Climate*, edited by W. H. Mathews, W. W. Kellog, and G. D. Robinson, pp. 141–155, M.I.T. Press, Cambridge, Mass., 1971.

NASA Langley Research Center, Data management system, the regional, zonal and global S-4 user's guide, 43 pp., Hampton, Va., 1985.

Pellerin, G., and R. Benoit, Surface geophysical fields, 34 pp., Can. Meteorol. Cent., Environ. Can., 1987.

Pinker, R. T., and I. Laszlo, Modeling surface solar irradiance for satellite applications on a global scale, *J. Appl. Meteorol.*, *31*, 194–211, 1992.

Ramanathan, V., The role of Earth radiation budget studies in climate and general circulation research, *J. Geophys. Res.*, *92*, 4075–4095, 1987.

Raschke, E., and H. J. Preuss, The determination of the solar radiation budget at the Earth's surface from satellite measurements, *Meteorol. Rundsch.*, *32*, 18–28, 1979.

Raschke, E., A. Gratzki, and M. Rieland, Estimates of global radiation at the ground from the reduced data sets of the International Satellite Cloud Climatology Project, *J. Climatol.*, *7*, 205–213, 1987.

Sasamori, T., J. London, and D. V. Hoyt, Radiation budget of the southern hemisphere, *Meteorol. Monogr.*, *13*(35), 1975.

Schmetz, J., Towards a surface radiation climatology: Retrieval of downward irradiances from satellites, *Atmos. Res.*, *23*, 287–321, 1989.

Suttles, J. T., and G. Ohring, Report of the workshop on surface radiation budget for climate applications, *Rep. WCRP*, *WCP-119*, *WMO/TD 109*, 144 pp., World Meteorol. Organ., Geneva, 1986.

U.S. National Academy of Sciences, Understanding climatic change, 14 pp., Washington, D. C., 1975.

Vowinckel, E., and S. Orvig, Energy balance of the Arctic, I, Incoming and absorbed solar radiation at the ground in the Arctic, *Arch. Meteorol. Geophys. Bioklimatol.*, *13*, 352–377, 1964.

Wallance, J. M., and P. V. Hobbs, *Atmospheric Science: An Introductory Survey*, 467 pp., Academic, San Diego, Calif., 1977.

Weare, B. C., Relationships between net radiation at the surface and the top of atmosphere derived from a general circulation model, *J. Clim.*, *2*, 193–197, 1989.

Wittman, G. D., Parameterization of the solar and infrared radiative properties of clouds, M.S. thesis, Dep. of Meteorol., Univ. of Utah, Salt Lake City, 1978.

H. G. Leighton, Department of Atmospheric and Oceanic Sciences, McGill University, 805 Sherbrooke W. St., Montreal, Quebec, Canada H3A 2K6.

Z. Li, Canada Centre for Remote Sensing, 588 Booth St., Ottawa, Ontario, Canada K1A 0Y7.

(Received May 15, 1992;
revised December 29, 1992;
accepted December 29, 1992.)